ACS APPLIED MATERIALS & INTERFACES

Research Article

Cite This: ACS Appl. Mater. Interfaces XXXX, XXX, XXX−XXX

www.acsami.org

Substrate-Independent Epitaxial Growth of the Metal−Organic Framework MOF-508a

M. Wilson,[†] S. N. Barrientos-Palomo,[†] P. C. Stevens,[†] N. L. Mitchell,[†] G. Oswald,[†] C. M. Nagaraja,[‡,§] and J. P. S. Badyal*[,†,§]

[†]Department of Chemistry, Science Laboratories, Durham University, Durham DH1 3LE, U.K.

[‡]Department of Chemistry, Indian Institute of Technology Ropar, Punjab 140001, India

ABSTRACT: Plasmachemical deposition is a substrate-independent method for the conformal surface functionalization of solid substrates. Structurally well-defined pulsed plasma deposited poly(1-allylimidazole) layers provide surface imidazole linker groups for the directed liquid-phase epitaxial (layer-by-layer) growth of metal−organic frameworks (MOFs) at room temperature. For the case of microporous [Zn (benzene-1,4-dicarboxylate)-(4,4′-bipyridine)$_{0.5}$] (MOF-508), the MOF-508a polymorph containing two interpenetrating crystal lattice frameworks undergoes orientated Volmer−Weber growth and displays CO_2 gas capture behavior at atmospheric concentrations in proportion to the number of epitaxially grown MOF-508 layers.

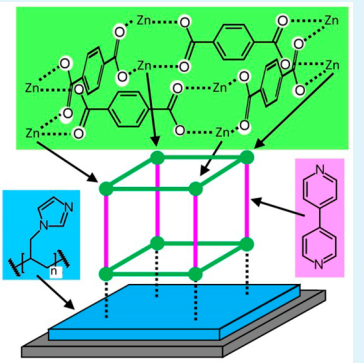

KEYWORDS: *metal−organic framework (MOF), epitaxial growth, surface functionalization, plasmachemical deposition, CO_2 capture, MOF coatings*

1. INTRODUCTION

Reticular synthesis of metal−organic frameworks (MOFs) entails the coordination bonding of a metal ion to organic ligand building blocks via self-assembly, leading to the formation of two- or three-dimensional structures.[1] Some of these can be highly porous (several thousand $m^2\ g^{-1}$), and they have been developed for a variety of applications including hydrogen storage,[2] gas and liquid separations,[3] catalysis,[4] and supercapacitors.[5] The wide range of organic linkers and metal cations available allows for the fine tuning of pore sizes[6] and chemical reactivity.[7] To this end, MOFs have been found to be promising candidates for CO_2 gas capture materials due to their pore size selective adsorption combined with their high internal surface areas.[8]

However, MOFs are mainly synthesized as particulate bulk materials, which can be difficult to handle or incorporate into specific device architectures. An alternative strategy is to grow MOFs directly onto a solid surface using liquid phase epitaxy (layer-by-layer). Previously, such surface-grown MOFs have been limited to specific substrate materials, including metals,[9−11] metal oxides,[11−14] self-assembled monolayers (SAMs),[15−19] and organic polymers.[20−24] The major drawback of these systems is that in each case the deposition technique needs to be tailored for the chosen substrate. Langmuir−Blodgett deposition of presynthesized MOF particles directly onto substrates has been explored as an alternative for CO_2 capture, but this approach lacks robustness due to the absence of any direct chemical coordination between the deposited MOF particles and the underlying substrate material.[25]

A particularly interesting MOF is [Zn (benzene-1,4-dicarboxylate)-(4,4′-bipyridine)$_{0.5}$] (MOF-508), which is reported to display high levels of CO_2 capture and separation of linear alkanes.[26,27] Its bulk form can be solvothermally synthesized by reacting benzene-1,4-dicarboxylic acid (terephthalic acid), 4,4′-bipyridine, and zinc nitrate in an organic solvent such as dimethylformamide at elevated temperatures (363 K).[26] The product MOF crystallites are built of zinc-terephthalate primitive square frameworks, separated by 4,4′-bipyridine pillars (Scheme 1). In its bulk form, the MOF framework is interpenetrated with a second identical framework (catenation), leading to a reduced pore size (4.0 Å diameter) and forming one of two polymorphs, MOF-508a and MOF-508b (which are solvent-inclusive and solvent-free materials, respectively).[26−28] Such a reduction in MOF network pore size improves CO_2 adsorption due to an increase in interactions with the MOF channel walls.[29]

Self-assembled monolayer liquid phase epitaxy of MOF-508 growth onto gold substrates is reported to give rise to the loss of MOF framework interpenetration, leading to only large pores (yielding reduced CO_2 capture efficiency as well as higher water contamination in humid environments).[15,28] In this article, we describe a methodology for the room temperature surface growth of MOF-508 materials by liquid phase epitaxy that leads to the formation of an interpenetrated MOF-508

Received: October 23, 2017
Accepted: January 4, 2018

DOI: 10.1021/acsami.7b16029
ACS Appl. Mater. Interfaces XXXX, XXX, XXX−XXX

Scheme 1. Layer-by-Layer Growth of MOF-508 onto a Pulsed Plasma Deposited Poly(1-allylimidazole) Linker Layer

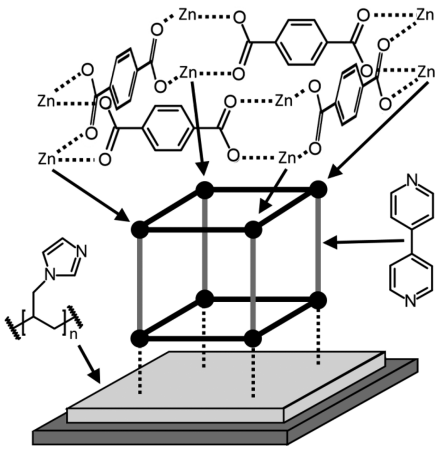

network with a reduced pore size (akin to MOF-508a, as evidenced by X-ray diffraction and infrared spectroscopy) and is therefore better suited to CO_2 capture and stability toward humidity. This comprises pulsed plasma deposition of a poly(1-allylimidazole) layer onto either quartz crystal microbalance (QCM) discs or polytetrafluorethylene (PTFE) membranes to generate surface linker imidazole groups, followed by liquid phase epitaxial growth of MOF-508 using zinc acetate as the metal ion source in association with terephthalic acid and 4,4′-bipyridine as secondary building units (Scheme 1). The pulsed plasma deposition step entails modulating an electrical discharge during the flow of gaseous 1-allylimidazole precursor (which contains a polymerizable carbon−carbon double bond[30,31]) over the substrate. Mechanistically, there are two distinct reaction regimes corresponding to the plasma duty cycle on and off periods (typical time scales are on the order of microseconds and milliseconds, respectively).[32] Namely, monomer activation and reactive site generation occur at the substrate surface during each short burst of plasma during the on period (via VUV irradiation, ion, or electron bombardment) followed by conventional carbon−carbon double bond polymerization proceeding in the subsequent extended off period (in the absence of any VUV-, ion-, or electron-induced damage to the growing film). High levels of precursor functional group structural retention within pulsed plasma deposited nanolayers can be achieved (as confirmed by XPS, ToF-SIMS, and NMR).[33] Strong covalent attachment of the deposited functional layers to the underlying substrate occurs via free radical sites created at the interface during electrical discharge ignition. Other distinct advantages of the plasma-chemical approach include the fact that it is quick (single-step), solventless, and energy-efficient, as well as the fact that the reactive gaseous nature of the electrical discharge provides three-dimensional conformality to the host substrate geometry.[34] The MOF-508 layers grown by liquid phase epitaxy onto pulsed plasma deposited poly(1-allylimidazole) functionalized materials in the present study have been tested for CO_2 capture in both pure CO_2 atmospheres as well as at diluted atmospheric concentrations.

2. EXPERIMENTAL SECTION

2.1. Pulsed Plasma Deposition of Poly(1-allylimidazole) Linker Layer. A cylindrical glass reactor (5.5 cm diameter, 475 cm^3 volume) housed within a Faraday cage was used for plasmachemical deposition. This was connected to a 30 L min^{-1} rotary pump (E2M2, Edwards Vacuum Ltd.) via a liquid nitrogen cold trap (base pressure less than 1.5×10^{-3} Torr and air leak rate better than 6×10^{-9} mol s^{-1}). A copper coil wound around the reactor (4 mm diameter, 10 turns, located 10 cm downstream from the gas inlet) was connected to a 13.56 MHz radio frequency (RF) power supply via an L−C matching network. A signal generator (model TG503, Thurlby Thandar Instruments Ltd.) was used to trigger the RF power supply. Prior to film deposition, the whole apparatus was thoroughly scrubbed using detergent and hot water, rinsed with propan-2-ol (+99.5 wt %, Fisher Scientific UK Ltd.), oven-dried at 423 K, and further cleaned using a 50 W continuous wave air plasma at 0.15 Torr pressure for 30 min.

Quartz crystal microbalance disc (14 mm diameter, gold coated, INFICON GmbH) and silicon substrate (Silicon Valley Microelectronics Inc.) preparation comprised successive 15 min sonication in propan-2-ol and then cyclohexane (+99.7 wt %, Sigma-Aldrich Co.) followed by insertion into the center of the chamber. Further cleaning entailed running a 50 W continuous wave air plasma at 0.15 Torr pressure for 15 min. This was followed by plasmachemical film deposition. In addition, PTFE membrane (180 ± 10 μm thickness, 5 ± 2 μm surface pore size determined by SEM, Mupor Ltd.) was used as a flexible substrate (the air plasma cleaning step was bypassed due to its polymeric nature).

A thin layer of tetramethylsilane plasma polymer (20 ± 7 nm) was deposited first in order to provide an organosilicon network for good adhesion to the substrate of the pulsed plasma deposited poly(1-allylimidazole) film.[35] Tetramethylsilane precursor (+99.9 wt %, Alfa Aesar, Thermo Fisher Scientific Inc.) was loaded into a sealable glass tube, degassed via several freeze−pump−thaw cycles, and then attached to the reactor. This was followed by purging the chamber with tetramethylsilane vapor at a pressure of 0.15 Torr for 15 min prior to electrical discharge ignition. Plasma deposition was performed in continuous wave mode using a RF generator power output of 3 W for 120 s. Upon plasma extinction, the tetramethylsilane vapor was allowed to continue to pass through the system for a further 15 min, and then the chamber was evacuated to base pressure followed by venting to atmosphere.

The tetramethylsilane plasma polymer coated substrates were then inserted into a cleaned chamber for pulsed plasma polymer deposition of the MOF linker layer. 1-Allylimidazole (+97 wt %, Acros Organics B.V.B.A.) precursor was loaded into a sealable glass tube, degassed via several freeze−pump−thaw cycles, and then attached to the reactor. Precursor vapor was then allowed to purge the apparatus at a pressure of 0.11 Torr for 15 min prior to electrical discharge ignition. Pulsed plasma deposition was performed using a duty cycle on period (t_{on}) of 20 μs and a duty cycle off period (t_{off}) of 1200 μs in conjunction with a RF generator power output (P_{on}) of 30 W for 15 min to give a film thickness of 243 ± 8 nm (thicker films of 1.69 ± 0.09 μm were obtained by longer deposition in order to match the sampling depth required for infrared spectroscopy RAIRS measurements).[36] Upon plasma extinction, the precursor vapor was allowed to continue to pass through the system for a further 15 min, and then the chamber was evacuated to base pressure followed by venting to atmosphere.

2.2. Growth of MOF-508 Layers. MOF-508 growth onto pulsed plasma deposited poly(1-allylimidazole) coated substrates was carried out by liquid phase epitaxy at room temperature (293 K).[15] A 1.0 mM zinc acetate (99.99 wt %, Sigma-Aldrich Co.) in tetrahydrofuran (99.8 wt %, Fisher Scientific UK Ltd.) solution was sonicated for 30 min prior to use. A second solution comprising 0.2 mM terephthalic acid (97 wt %, Sigma-Aldrich Co.) and 0.2 mM 4,4′-bipyridine (98 wt %, Sigma-Aldrich Co.) in tetrahydrofuran was also sonicated for 30 min prior to use. The linker-coated substrates were immersed into the zinc acetate solution for 5 min, rinsed in fresh tetrahydrofuran for 10 s, and dried in air for 1 min (PTFE substrates used a 2 min drying period). Once dry, the coated substrates were immersed into the terephthalic acid-4,4′-bipyridine solution for 5 min, followed by rinsing in fresh tetrahydrofuran for 10 s and drying in air. This is designated as one complete liquid phase epitaxy cycle and corresponds to one layer of

DOI: 10.1021/acsami.7b16029
ACS Appl. Mater. Interfaces XXXX, XXX, XXX−XXX

the MOF; the cycle was repeated multiple times to build up the required number of layers. This procedure led to solvent incorporation to give MOF-508a (as determined by X-ray diffraction). Activation of this material (solvent removal) was achieved by employing a low boiling point solvent (tetrahydrofuran) during the MOF synthesis, which readily desorbs out of the MOF lattice under vacuum to leave behind open cavities available for CO_2 capture.[37]

2.3. Film Characterization. Infrared spectra were acquired using an FTIR spectrometer (Spectrum One, PerkinElmer Inc.) fitted with a liquid nitrogen cooled MCT detector operating at 4 cm^{-1} resolution across the 400−4000 cm^{-1} range. For reflection−absorption infrared (RAIRS) spectra of pulsed plasma deposited poly(1-allylimidazole) and grown MOF layers, a variable angle reflection−absorption accessory (Specac Ltd.) was adjusted to a grazing angle of 66° for silicon wafer substrates and p-polarization. Attenuated total reflectance (ATR) infrared spectra of 1-allylimidazole liquid precursor and MOF-508 starting materials were obtained using a Golden Gate accessory (Specac Ltd.)

Surface elemental compositions were measured by X-ray photoelectron spectroscopy (XPS) using a VG ESCALAB II electron spectrometer equipped with a nonmonochromated Mg $K\alpha_{1,2}$ X-ray source (1253.6 eV) and a concentric hemispherical analyzer. Photoemitted electrons were collected at a takeoff angle of 20° from the substrate normal, with electron detection in the constant analyzer energy mode (CAE, pass energies of 20 and 50 eV for high resolution and survey spectra, respectively). Experimentally determined instrument sensitivity factors were C(1s)/O(1s)/N(1s) = 1.00:0.35:0.70. The core level binding energy envelopes were fitted using Gaussian peak shapes with fixed full-width at half maxima and linear backgrounds.[38] All binding energy values are referenced to the C(1s) hydrocarbon ($-\underline{C}_xH_y$) peak at 285.0 eV.[39]

X-ray diffractograms were acquired with a powder diffractometer (model d8, Bruker Corp.) across the 5−80° 2θ range using a 0.02° step size. The copper anode X-ray source (Cu Kα 1.5418 Å wavelength radiation) was operated at 40 kV and 40 mA.

Scanning electron microscopy (SEM) analysis was undertaken using secondary electron detection mode, in conjunction with a 25 kV accelerating voltage (model VEGA3 LMU SEM, Tescan Orsay Holding, a.s.).

2.4. CO_2 Gas Capture. CO_2 adsorption onto coated quartz crystal microbalance substrates (Front Load Single Sensor, INFICON GmbH) housed inside a glass chamber was carried out at 293 K. The sensor was connected to a thin film deposition monitor (model XTM/2, INFICON GmbH). Each coated quartz crystal microbalance disc was loaded into the chamber and evacuated at 4×10^{-2} Torr for 24 h at 293 K, leading to the desorption of entrapped MOF-508a lattice solvent molecules.[37] In order to mimic the equivalent concentration at atmospheric pressure, CO_2 gas (99.995 vol %, BOC Ltd.) was introduced to the system at 0.2 Torr pressure, followed by a dry 80:20 O_2 (99.5 vol %, BOC Ltd.)/N_2 (99.998 vol %, BOC Ltd.) gas mixture (<60 ppm of H_2O, Series 3 moisture monitor, GE Panametrics Ltd.) to make up to 760 Torr total pressure. Adsorbed CO_2 gas mass readings were taken at set intervals over a 456 h period and normalized to the flat area of the quartz crystal microbalance disc (1.54 cm^2). Control experiments using 760 Torr of dry 80:20 oxygen/nitrogen gas mix (no CO_2) showed no mass change.

Volumetric CO_2 gas adsorption for flexible PTFE supported MOF layers was carried out in a sorptometer (model BET-201, Porous Materials Inc.). Samples were loaded into a glass tube of known volume and degassed at $<1 \times 10^{-2}$ Torr for 24 h to remove any adsorbed moisture. CO_2 gas was introduced into a calibrated volume at 1000 ± 2 Torr at 293 K, followed by equilibration with the sample chamber to provide an initial CO_2 pressure over the sample of 720 ± 2 Torr. Pressure readings were taken at fixed intervals over a period of 480 h in order to follow the pressure drop as a function of time. The number of moles of adsorbed gas was calculated from the pressure drop in the system (for which the volume is known), which is then converted to mass of adsorbed CO_2 gas, and normalized to the size of the flat area of the PTFE membrane (40.5 cm^2). The sample volume was calculated by gas pycnometry using N_2 gas and was subtracted from the sample cell volume for CO_2 adsorption measurements.

3. RESULTS

3.1. Pulsed Plasma Deposition of a Poly(1-allylimidazole) Linker Layer. Infrared spectroscopy of pulsed plasma deposited poly(1-allylimidazole) films confirmed a high level of precursor imidazole functional group structural retention[36] (Figure 1). Characteristic imidazole ring absorbances include

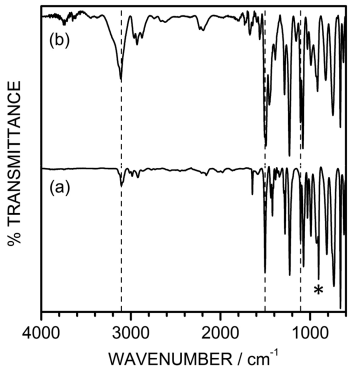

Figure 1. Infrared spectroscopy: (a) ATR of liquid 1-allylimidazole precursor and (b) RAIRS of pulsed plasma poly(1-allylimidazole) deposited onto a silicon wafer. *Denotes monoalkyl vinyl $=CH_2$ wag vibration at 906 cm^{-1} in 1-allylimidazole precursor. Dashed lines denote characteristic imidazole ring absorbances at 3107, 1504, and 1107 cm^{-1}. Overall relative intensity differences between the two spectra are due to the use of ATR versus RAIRS infrared spectroscopic techniques.[45]

the C=C−H ring stretch (3107 cm^{-1}), C=N ring stretch (1504 cm^{-1}), and N=C−H ring in-plane bend (1107 cm^{-1}) vibrations.[40] Disappearance of the monoalkyl vinyl $=CH_2$ wag vibration mode (906 cm^{-1}) associated with the 1-allylimidazole precursor molecule is consistent with selective polymerization of the vinyl group during pulsed plasma deposition.[41] Absorbance bands visible in the 1560−1700 cm^{-1} spectral range can be attributed to a small amount of electrical discharge fragmented imidazole group C=N stretches,[42] and carbonyl stretches belonging to adducts formed through atmospheric carbon dioxide adsorption following exposure of the deposited film to air.[43,44]

XPS analysis of pulsed plasma poly(1-allylimidazole) deposited onto a silicon wafer detected only carbon, nitrogen, and low levels of oxygen (attributed to a small amount of water adsorption and adducts formed through carbon dioxide adsorption upon air exposure[42,43]). The N(1s) binding envelope could be fitted to two different nitrogen environments at 398.7 and 400.5 eV, corresponding to the imidazole ring C=$\underline{N}$ and C—$\underline{N}$ nitrogen centers, respectively[46] (Figure 2). Their slight deviation in relative concentrations away from the expected theoretical 1:1 peak area ratio for the imidazole ring structure stems from a low level of precursor fragmentation occurring within the electrical discharge.[42] The C(1s) and O(1s) XPS regions comprised single overall peak shapes and were therefore unresolvable.

3.2. Epitaxial Growth of MOF-508 Layers. The infrared spectrum of 200 layer MOF-508 grown by liquid phase epitaxy onto a pulsed plasma poly(1-allylimidazole) coated silicon wafer contains two strong, broad absorbances between 1400 and 1700 cm^{-1}, which can be respectively attributed to the

DOI: 10.1021/acsami.7b16029
ACS Appl. Mater. Interfaces XXXX, XXX, XXX−XXX

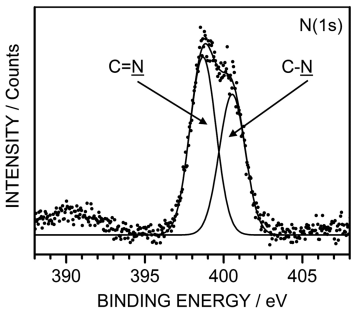

Figure 2. N(1s) XPS spectrum of pulsed plasma poly(1-allylimidazole) deposited onto a silicon wafer. Weak Mg Kα_3 and Mg Kα_4 X-ray satellites are, respectively, 8.4 and 10.1 eV lower in binding energy relative to assigned Mg K$\alpha_{1,2}$ components.

overlapping terephthalate C−O$^-$ deformation vibration (slightly shifted to lower wavenumbers from 1406 cm^{-1} in terephthalic acid for C−OH due to proton loss[47,48]) and carbonyl stretch vibration (the terephthalic acid 1673 cm^{-1} feature is shifted to 1670 cm^{-1} due to metal coordination[47,49]) (Figure 3 and Table 1). Also, there are the 4,4′-bipyridine ring

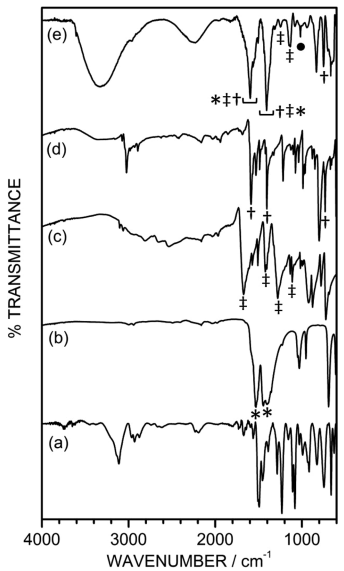

Figure 3. Infrared spectra: (a) pulsed plasma poly(1-allylimidazole) deposited onto a silicon wafer; (b) zinc acetate; (c) terephthalic acid; (d) 4,4′-bipyridine; and (e) 200 layer MOF-508 grown onto pulsed plasma poly(1-allylimidazole) coated silicon wafer. Fingerprint peaks: (*) zinc acetate, (‡) terephthalic acid, (†) 4,4′-bipyridine, and (•) tetrahydrofuran. See Table 1 for assignments.

quadrant vibration (1593 cm^{-1} shifted to higher wavenumbers due to coordination relative to 1585 cm^{-1} for 4,4′-bipyridine)[50,51] and the 4,4′-bipyridine semicircle stretch vibration (1408 cm^{-1}).[50] These infrared spectral features are consistent with the incorporation of both terephthalate and 4,4′-bipyridine organic linkers during the layered growth of MOF-508 (Scheme 1). Bulk MOF-508 is also reported to display these strong infrared absorbances.[52] Additional lower intensity vibrations include C−O$^-$ deformation mode (shifted to 1250 cm^{-1} compared to 1276 cm^{-1} for C−OH in terephthalic acid due to proton loss),[47,48] substituted benzene C−H deformation mode (1134 cm^{-1}) for the constituent terephthalate linker, and pyridine sextant out-of-plane bend vibration (748 cm^{-1}) for the constituent 4,4′-bipyridine linker unit.[47,50] The low intensity peak at 1017 cm^{-1} can be assigned to the antisymmetric C−O−C valence vibration of lattice incorporated tetrahydrofuran solvent molecules, which is consistent with the formation of the solvent-inclusive MOF-508a polymorph.[53]

Powder X-ray diffractograms of 200 layer MOF-508 grown onto a pulsed plasma poly(1-allylimidazole) coated silicon wafer showed two prominent peaks at low detector angles that are consistent with an orientated large lattice constant material (Figure 4). These diffraction peaks at 6.3 and 12.5° are assigned to the (001) and (002) planes of the solvent-inclusive MOF (MOF-508a), with calculated lattice spacings of 14.0 and 7.1 Å, respectively.[15,26] A lack of strong intensities for the (100) and (010) MOF-508a diffraction peaks indicates that the majority of the MOF crystallites have been templated (orientated) by the pulsed plasma deposited poly(1-allylimidazole) surface. The greater intensity of the (001) peak compared to the (002) peak supports an interpenetrated network of MOF-508a, which is caused by the incorporation of a second lattice.[15,55,56] This should be contrasted against noninterpenetrated MOF-508, which is reported to show the reverse (001) to (002) peak intensity ratio due to the absence of destructive interference effects (as confirmed by comparing experimental versus calculated X-ray diffraction patterns for MOF-508a, MOF-508b).[15] The two low intensity 2θ peak values between 8 and 10° are attributable to a small amount of nonorientated solvent-inclusive MOF-508a and solvent-free MOF-508b, respectively.[15]

Scanning electron micrographs taken following 20 and 200 layer growth of MOF-508 onto a pulsed plasma poly(1-allylimidazole) coated silicon wafer show the presence of individual crystallites on the surface (Figure 5). Upon reaching 200 layers of MOF-508 growth, a clear crystallite morphology is visible, which is consistent with the bulk MOF-508 triclinic unit cell.[26] This confirms that imidazole linker group functionalized substrate surface provides seeding sites for the layer-by-layer growth of MOF-508 crystallites. The direction of crystal growth was vertically outward, but they were not aligned within the plane of the substrate. The epitaxially grown MOF-508 crystallites were found to be strongly bonded to the underlying substrate (as evidenced by prolonged rinsing and agitation in tetrahydrofuran solvent).

3.3. CO_2 Gas Capture. MOF-508 layers grown onto pulsed plasma poly(1-allylimidazole) coated quartz crystal microbalance (QCM) discs were studied for CO_2 adsorption capacity at the equivalent of atmospheric CO_2 partial pressures (0.3 Torr CO_2 diluted in a 20:80 O_2/N_2 gas mixture to give 760 Torr total pressure[57]) (Figure 6). Adsorption of CO_2 was rapid during the first 24 h, followed by a more gradual rise over the next 10 days. The overall capacity for CO_2 adsorption correlated to the number of MOF-508 layers grown (Figure 6). This is consistent with there being deposition of a single MOF-508 layer during each liquid phase epitaxial growth cycle. Saturation of gas adsorption was measured by using 760 Torr pressure of CO_2, and this showed that the maximum CO_2 adsorption capacity of the 20 layer MOF-508 was reached after 456 h, which was only 10% greater than the amount of CO_2 adsorbed at 0.3 Torr CO_2 partial pressure (after 456 h) (Figure 7). This relative insensitivity of CO_2 adsorption versus CO_2 partial pressure is consistent with earlier bulk MOF-508 studies[26] and demonstrates the high affinity of the grown MOF-508 layers toward CO_2 gas capture across a wide range of

DOI: 10.1021/acsami.7b16029
ACS Appl. Mater. Interfaces XXXX, XXX, XXX−XXX

Table 1. Infrared Spectral Assignments of MOF-508 Constituent Building Units and 200 Layer MOF-508 Grown onto Pulsed Plasma Deposited Poly(1-allylimidazole)[a]

	absorbance/cm^{-1}			
assignment	zinc acetate	terephthalic acid	4,4′-bipyridine	200 layers of MOF-508
carbonyl symmetric stretch[54]	1443	–	–	ca. 1430
carbonyl asymmetric stretch[54]	1531	–	–	ca. 1530
substituted benzene C–H deformation[47]		1138		1134
carboxylic acid C–OH/[C–O$^-$] deformation[47,48]	–	1276	–	[1250]
carboxylic acid C–OH/[C–O$^-$] deformation[47,48]	–	1406	–	[ca. 1400]
carboxylic acid carbonyl stretch[47]	–	1673	–	ca. 1670
pyridine sextant out-of-plane bend[50]	–	–	734	748
pyridine semicircle stretch[50]	–	–	1402	1408
pyridine quadrant stretch[50,51]	–	–	1585	1593
tetrahydrofuran solvent antisymmetric C–O–C vibration[53]				1017

[a]Pulsed plasma deposited poly(1-allylimidazole) assignments are given in Figure 1. Other absorbances include the C–H stretch (ca. 3100 cm^{-1}), background water O–H stretch (ca. 3300 cm^{-1}), and background carbon dioxide C–O stretch (ca. 2300 cm^{-1}).[47]

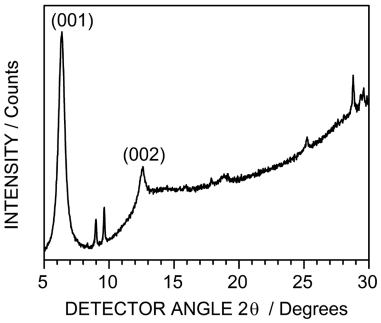

Figure 4. Powder XRD of 200 layer MOF-508 grown onto a pulsed plasma poly(1-allylimidazole) coated silicon wafer. The two low intensity 2θ peak values between 8 and 10° are attributable to a small amount of nonorientated solvent-inclusive MOF-508a and solvent-free MOF-508b, respectively, based upon the corresponding bulk phase XRD patterns.[15]

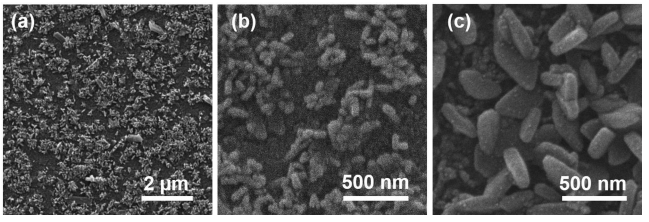

Figure 5. SEM micrographs of MOF-508 crystallite growth onto a pulsed plasma poly(1-allylimidazole) coated silicon wafer substrate: (a, b) 20 layers and (c) 200 layers.

partial pressures. Control experiments using pulsed plasma poly(1-allylimidazole) coated QCM discs showed a low level of CO_2 adsorption (due to adduct formation with imidazole centers)[43,44] (Figure 6).

The practical viability of the described methodology for preparing CO_2 capture MOF materials supported on different types of substrate was demonstrated further by translating the developed methodology to flexible PTFE membrane films (Figure 8). PTFE supported 20 layer MOF-508 captured 148 μg cm^{-2} of CO_2 following 480 h of CO_2 gas exposure. The rate of CO_2 uptake over the first 12 h (starting from 2 min after the initial exposure) was 1.51 ± 0.10 μg cm^{-2} h^{-1} (which is

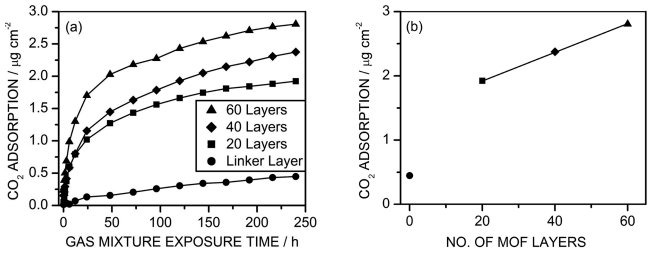

Figure 6. Quartz crystal microbalance CO_2 gas capture using 0.3 Torr partial pressure of CO_2 gas diluted in a 20:80 O_2/N_2 gas mixture to give 760 Torr total pressure as a function of (a) gas mixture exposure time and (b) number of MOF-508 layers grown onto pulsed plasma deposited poly(1-allylimidazole) (cm^{-2} refers to the surface area of the quartz crystal microbalance disc).

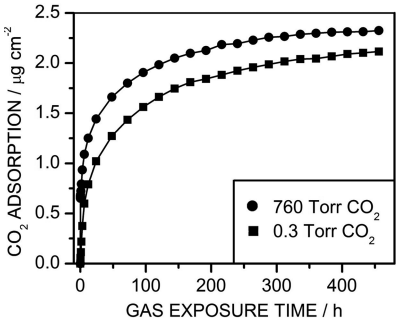

Figure 7. Quartz crystal microbalance CO_2 gas capture as a function of exposure time for 20 layer MOF-508 grown onto pulsed plasma deposited poly(1-allylimidazole) using (■) 0.3 Torr partial pressure of CO_2 gas diluted in a 20:80 O_2/N_2 gas mixture to give 760 Torr total pressure and (●) 760 Torr of CO_2 gas (cm^{-2} refers to the surface area of the quartz crystal microbalance disc).

significant given the ultrathin nature of the 20 layer MOF), compared to 0.51 ± 0.04 μg cm^{-2} h^{-1} for the uncoated PTFE membrane reference (no MOF or linker layer and just PTFE pore absorption[58]). Slower CO_2 gas adsorption was observed for these PTFE supported MOF-508 layers compared to their quartz crystal microbalance counterparts. This can be attributed to a combination of a lower starting pressure in the volumetric adsorption system (720 Torr compared to 760 Torr for QCM

DOI: 10.1021/acsami.7b16029
ACS Appl. Mater. Interfaces XXXX, XXX, XXX–XXX

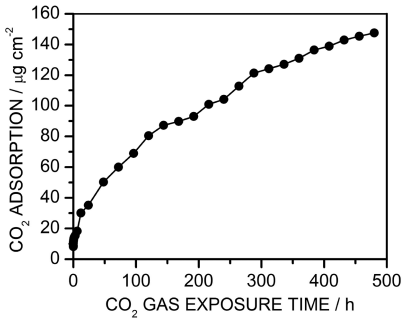

Figure 8. Mass of CO_2 gas adsorbed by 20 layer MOF-508 grown onto a pulsed plasma deposited poly(1-allylimidazole) coated PTFE membrane in a sealed CO_2 atmosphere (initial pressure 720 Torr) as a function of exposure time (calculated from volumetric gas adsorption measurements; cm^{-2} refers to the size of the piece of PTFE membrane substrate).

studies) and a larger pressure drop over time due to the greater gas adsorption capacity of the PTFE membrane supported MOF-508 material, resulting in a longer period of time to reach equilibrium between $CO_{2(g)}$ versus $CO_{2(ads)}$ (Figures 7 and 8). The difference in adsorbed mass of CO_2 after 456 h between QCM and PTFE supported materials (2.1 and 145 $\mu g\ cm^{-2}$, respectively) is due to the higher internal surface area of the porous PTFE membrane available for MOF crystallite growth.

4. DISCUSSION

Pulsed plasmachemical functionalization of solid surfaces using polymerizable functional precursors is a well-established, solventless, single-step, conformal, and substrate-independent technique that offers the advantage of high levels of functional group retention, thus making it well-suited for the deposition of functional groups onto both inorganic and organic substrates for MOF templating. Infrared spectroscopy and XPS analyses have shown that there is a large degree of imidazole ring retention during pulsed plasma deposition of 1-allylimidazole precursor, which is a prerequisite for the epitaxial growth of MOF-508 layers (Figures 1 and 2).

MOF-508a was found to grow selectively onto the pulsed plasma poly(1-allylimidazole) deposited layers, thereby confirming the substrate-independent nature of the methodology. The crystallite morphology observed by SEM is consistent with other liquid phase epitaxial grown MOF layers (which display a Volmer–Weber island layer-by-layer growth mechanism[19]) (Figure 5). This indicates that the surface energy of the crystal–solution interface is greater than that of the substrate–solution interface, which leads to the growth of three-dimensional islands on the surface (rather than Frank–van der Merwe uniform layer-by-layer growth across the whole substrate).[59]

In contrast to the previously reported growth of MOFs onto self-assembled monolayers (SAMs; which provide templating of noninterpenetrated MOF-508 lattice[15]), the pulsed plasma deposited layer approach gives rise to interpenetrated MOF-508 lattices (MOF-508a), providing the added benefit of an appropriate pore size for selective CO_2 adsorption (4.0 Å diameter) and stability toward water uptake from ambient humidity.[26,28] Also, in this case, the Volmer–Weber island layer-by-layer growth mechanism provides relatively less compact packing of the MOF-508a crystallites (higher external surface area), giving guest CO_2 molecules greater access to MOF-508a crystallite pore openings from the (100) and (010) faces (which are blocked for both SAM-based close-packed unidirectional and perfect Frank–van der Merwe (001) layer-by-layer MOF film growth modes[60,61]). Such orientation specific gas adsorption behaviors have been documented for other MOF systems.[62]

Assuming complete coverage of an underlying flat substrate with a single unit cell thickness of interpenetrated MOF-508 layer during each epitaxial cycle, the maximum theoretical mass of MOF-508a grown onto the pulsed plasma deposited poly(1-allylimidazole) layer coated quartz crystal microbalance substrates is calculated to be 16.0 μg after 60 cycles (based on the MOF-508a unit cell dimensions measured by XRD and the QCM disc area). Using this value in conjunction with the experimental QCM CO_2 gas uptake measurements, the total amount of CO_2 captured per gram of MOF-508a is calculated to be 6 mmol g^{-1}; in fact, the incomplete layer-by-layer coverage of the substrate with MOF (due to the Volmer–Weber island growth mechanism) means that this value is an underestimate. This CO_2 uptake value (6 mmol g^{-1}) is comparable to previously reported surface supported CO_2 capture MOFs (1–4 mmol g^{-1}) and bulk MOF-508 CO_2 capture materials (1–2 mmol g^{-1} at atmospheric pressure).[25,27,63] Furthermore, it appears to be on the same order of magnitude as other CO_2 sequestration technologies, such as alkali metal carbonates (9.4 mmol g^{-1})[64] and hyperbranched aminosilicas (5.5 mmol g^{-1}).[65] On the basis of this saturated QCM CO_2 gas adsorption value of 6 mmol g^{-1}, the CO_2/Zn(II) ratio is calculated to be 2:1 for the MOF-508a film, with fast adsorption occurring up to 50% gas uptake attributable to the interaction of CO_2 with vacant Zn(II) lattice coordination sites.[66] The gas adsorption rate slows beyond a CO_2/Zn(II) stoichiometric ratio of 1:1, which is attributable to the participation of secondary weaker adsorption sites and CO_2–CO_2 interactions becoming dominant.[66]

The practical viability of the pulsed plasma deposited poly(1-allylimidazole) templated MOF-508a layers for CO_2 capture under atmospheric conditions (diluted CO_2 concentrations in O_2/N_2 carrier gas mixture) has been demonstrated by achieving gas uptake values close to those measured at the saturation adsorption limit for a pure CO_2 atmosphere (Figure 7). High affinity for the separation of CO_2 at atmospheric concentrations from air has been previously reported for sodium hydroxide,[67] zeolites,[68] and some bulk MOFs,[69] but not for surface-anchored MOFs. By combining the aforementioned CO_2 adsorption properties with a plasmachemical deposited flexible substrate linker layer, the described approach facilitates the application of MOF-508 to a wide variety of substrate materials and geometries (including membranes and fibers) and hence CO_2 capture applications (for example, carbon sequestration, industrial flue gas scrubbers, and recirculating breathing apparatus), something which is not easily feasible using other surface-templating methods, such as self-assembled monolayers (SAMs), metals, or metal oxides due to their inherent substrate specificities. Furthermore, apart from host–guest interactions, the growth of such supported functional MOF layers could form the basis of physical or chemical responsive materials including phase transitions triggered by guest adsorption/desorption or photochemical, thermal, and mechanical stimuli.[70]

5. CONCLUSIONS

Pulsed plasma deposited poly(1-allylimidazole) layers can be used for the substrate-independent epitaxial growth of

DOI: 10.1021/acsami.7b16029
ACS Appl. Mater. Interfaces XXXX, XXX, XXX–XXX

microporous [Zn (benzene-1,4-dicarboxylate)-(4,4′-bipyridine)$_{0.5}$] (MOF-508) layers at room temperature. The observed surface crystallite morphology is consistent with the Volmer−Weber island layer-by-layer epitaxial growth mechanism. These MOF-508 layers display a high affinity toward the separation of carbon dioxide at atmospheric concentrations from oxygen/nitrogen carrier gas mixtures, and the total carbon dioxide capture capacity is found to correlate to the number of MOF-508 layers grown.

AUTHOR INFORMATION

Corresponding Author

*E-mail: j.p.badyal@durham.ac.uk

ORCID

C. M. Nagaraja: 0000-0002-4271-6424

J. P. S. Badyal: 0000-0002-5086-5737

Author Contributions

§C.M.N. and J.P.S.B. contributed equally to this work.

Notes

The authors declare no competing financial interest.

Data created during this research can be accessed at https://collections.durham.ac.uk.

ACKNOWLEDGMENTS

This work was supported by Engineering and Physical Sciences Research Council (EPSRC) grant reference EP/J005401/1 and studentship reference EP/502832/1. S. N. Barrientos-Palomo was funded by Consejo Nacional de Ciencia y Tecnología, Mexico (CONACyT), scholarship reference 409090. We thank T. Davey of the Electron Microscopy Research Services at Newcastle University.

REFERENCES

(1) Seth, S.; Matzger, A. Metal−Organic Frameworks: Examples, Counterexamples, and an Actionable Definition. *Cryst. Growth Des.* **2017**, *17*, 4043−4048.

(2) Rosi, N. L.; Eckert, J.; Eddaoudi, M.; Vodak, D. T.; Kim, J.; O'Keeffe, M.; Yaghi, O. M. Hydrogen Storage in Microporous Metal-Organic Frameworks. *Science* **2003**, *300*, 1127−1129.

(3) Li, J.-R.; Sculley, J.; Zhou, H.-C. Metal-Organic Frameworks for Separations. *Chem. Rev.* **2012**, *112*, 869−932.

(4) Liu, J.; Chen, L.; Cui, H.; Zhang, J.; Zhang, Li; Su, C.-Y. Applications of Metal−Organic Frameworks in Heterogeneous Supramolecular Catalysis. *Chem. Soc. Rev.* **2014**, *43*, 6011−6061.

(5) Sheberla, D.; Bachman, J. C.; Elias, J S.; Sun, C.-J.; Shao-Horn, Y.; Dincă, M. Conductive MOF Electrodes for Stable Supercapacitors with High Areal Capacitance. *Nat. Mater.* **2017**, *16*, 220−224.

(6) Du, L.; Lu, Z.; Zheng, K.; Wang, J.; Zheng, X.; Pan, Y.; You, X.; Bai, J. Fine-Tuning Pore Size by Shifting Coordination Sites of Ligands and Surface Polarization of Metal−Organic Frameworks To Sharply Enhance the Selectivity for CO_2. *J. Am. Chem. Soc.* **2013**, *135*, 562−565.

(7) Tanabe, K. K.; Cohen, S. M. Postsynthetic Modification of Metal−Organic Frameworks—a Progress Report. *Chem. Soc. Rev.* **2011**, *40*, 498−519.

(8) Li, J.-R.; Ma, Y.; McCarthy, M. C.; Sculley, J.; Yu, J.; Jeong, H.-K.; Balbuena, P. B.; Zhou, H.-C. Carbon Dioxide Capture-Related Gas Adsorption and Separation in Metal-Organic Frameworks. *Coord. Chem. Rev.* **2011**, *255*, 1791−1823.

(9) Zou, X.; Zhu, G.; Hewitt, I. L.; Sun, F.; Qiu, S. Synthesis of a Metal−Organic Framework Film by Direct Conversion Technique for VOCs Sensing. *Dalton Trans.* **2009**, *16*, 3009−3013.

(10) Ameloot, R.; Pandey, L.; Van der Auweraer, M.; Alaerts, L.; Sels, B. F.; De Vos, D. E. Patterned Film Growth of Metal-Organic Frameworks Based on Galvanic Displacement. *Chem. Commun.* **2010**, *46*, 3735−3737.

(11) Pan, C.; Nan, J.; Dong, X.; Ren, X.-M.; Jin, W. A Highly Thermally Stable Ferroelectric Metal-Organic Framework and Its Thin Film with Substrate Surface Nature Dependent Morphology. *J. Am. Chem. Soc.* **2011**, *133*, 12330−12333.

(12) Ahrenholtz, S. R.; Epley, C. C.; Morris, A. J. Solvothermal Preparation of an Electrocatalytic Metalloporphyrin MOF Thin Film and its Redox Hopping Charge-Transfer Mechanism. *J. Am. Chem. Soc.* **2014**, *136*, 2464−2472.

(13) Khaletskaya, K.; Turner, S.; Tu, M.; Wannapaiboon, S.; Schneemann, A.; Meyer, R.; Ludwig, A.; Van Tendeloo, G.; Fischer, R. A. Self-Directed Localization of ZIF-8 Thin Film Formation by Conversion of ZnO Nanolayers. *Adv. Funct. Mater.* **2014**, *24*, 4804−4811.

(14) Yoo, Y.; Jeong, H.-K. Rapid Fabrication of Metal Organic Framework Thin Films Using Microwave-Induced Thermal Deposition. *Chem. Commun.* **2008**, *21*, 2441−2443.

(15) Shekhah, O.; Wang, H.; Paradinas, M.; Ocal, C.; Schüpbach, B.; Terfort, A.; Zacher, D.; Fischer, R. A.; Wöll, C. Controlling Interpenetration in Metal−Organic Frameworks by Liquid-Phase Epitaxy. *Nat. Mater.* **2009**, *8*, 481−484.

(16) Otsubo, K.; Haraguchi, T.; Sakata, O.; Fujiwara, A.; Kitagawa, H. Step-by-Step Fabrication of a Highly Oriented Crystalline Three-Dimensional Pillared-Layer-Type Metal−Organic Framework Thin Film Confirmed by Synchrotron X-ray Diffraction. *J. Am. Chem. Soc.* **2012**, *134*, 9605−9608.

(17) Hinterholzinger, F. M.; Wuttke, S.; Roy, P.; Preuße, T.; Schaate, A.; Behrens, P.; Godt, A.; Bein, T. Highly Oriented Surface-Growth and Covalent Dye Labelling of Mesoporous Metal−Organic Frameworks. *Dalton Trans.* **2012**, *41*, 3899−3901.

(18) Hanke, M.; Arslan, H. K.; Bauer, S.; Zybaylo, O.; Christophis, C.; Gliemann, H.; Rosenhahn, A.; Wöll, C. The Biocompatibility of Metal−Organic Framework Coatings: An Investigation on the Stability of SURMOFs with Regard to Water and Selected Cell Culture Media. *Langmuir* **2012**, *28*, 6877−6884.

(19) Ohnsorg, M. L.; Beaudoin, C. K.; Anderson, M. E. Fundamentals of MOF Thin Film Growth via Liquid-Phase Epitaxy: Investigating the Initiation of Deposition and the Influence of Temperature. *Langmuir* **2015**, *31*, 6114−6121.

(20) Mao, Y.; Li, J.; Cao, W.; Ying, Y.; Sun, L.; Peng, X. Pressure-Assisted Synthesis of HKUST-1 Thin Film on Polymer Hollow Fiber at Room Temperature toward Gas Separation. *ACS Appl. Mater. Interfaces* **2014**, *6*, 4473−4479.

(21) Lu, C.; Ben, T.; Xu, S.; Qiu, S. Electrochemical Synthesis of a Microporous Conductive Polymer Based on a Metal−Organic Framework Thin Film. *Angew. Chem., Int. Ed.* **2014**, *53*, 6454−6458.

(22) Meilikhov, M.; Yusenko, K.; Schollmeyer, E.; Mayer, C.; Buschmann, H.-J.; Fischer, R. A. Stepwise Deposition of Metal Organic Frameworks on Flexible Synthetic Polymer Surfaces. *Dalton Trans.* **2011**, *40*, 4838−4841.

(23) Centrone, A.; Yang, Y.; Speakman, S.; Bromberg, L.; Rutledge, G. C.; Hatton, T. A. Growth of Metal-Organic Frameworks on Polymer Surfaces. *J. Am. Chem. Soc.* **2010**, *132*, 15687−15691.

(24) Zhou, M.; Li, J.; Zhang, M.; Wang, H.; Lan, Y.; Wu, Y.-N.; Li, F.; Li, G. A Polydopamine Layer as the Nucleation Center of MOF Deposition on "Inert" Polymer Surfaces to Fabricate Hierarchically Structured Porous Films. *Chem. Commun.* **2015**, *51*, 2706−2709.

(25) Benito, J.; Sorribas, S.; Lucas, I.; Coronas, J.; Gascon, I. Langmuir−Blodgett Films of the Metal−Organic Framework MIL-101(Cr): Preparation, Characterization, and CO_2 Adsorption Study Using a QCM-Based Setup. *ACS Appl. Mater. Interfaces* **2016**, *8*, 16486−16492.

(26) Chen, B.; Liang, C.; Yang, J.; Contreras, D. S.; Clancy, Y. L.; Lobkovsky, E. B.; Yaghi, O. M.; Dai, S. A Microporous Metal−Organic Framework for Gas-Chromatographic Separation of Alkanes. *Angew. Chem., Int. Ed.* **2006**, *45*, 1390−1393.

(27) Bastin, L.; Bárcia, P. S.; Hurtado, E. J.; Silva, J. A. C.; Rodrigues, A. E.; Chen, B. A Microporous Metal-Organic Framework for

DOI: 10.1021/acsami.7b16029
ACS Appl. Mater. Interfaces XXXX, XXX, XXX−XXX

Separation of CO_2/N_2 and CO_2/CH_4 by Fixed-Bed Adsorption. *J. Phys. Chem. C* **2008**, *112*, 1575−1581.
(28) Jasuja, H.; Walton, K. Effect of Catenation and Basicity of Pillared Ligands on the Water Stability of MOFs. *Dalton Transactions* **2013**, *42*, 15421−15426.
(29) Du, L.; Lu, Z.; Zheng, K.; Wang, J.; Zheng, X.; Pan, Yi.; You, X.; Bai, J. Fine-Tuning Pore Size by Shifting Coordination Sites of Ligands and Surface Polarization of Metal−Organic Frameworks to Sharply Enhance the Selectivity for CO_2. *J. Am. Chem. Soc.* **2013**, *135*, 562−565.
(30) Yasuda, H.; Hsu, T. Some Aspects of Plasma Polymerization Investigated by Pulsed R.F. Discharge. *J. Polym. Sci., Polym. Chem. Ed.* **1977**, *15*, 81−97.
(31) Savage, C. R.; Timmons, R. B.; Lin, J. W. Molecular Control of Surface Film Compositions Via Pulsed Radio-Frequency Plasma Deposition of Perfluoropropylene Oxide. *Chem. Mater.* **1991**, *3*, 575−577.
(32) Ryan, M. E.; Hynes, A. M.; Badyal, J. P. S. Pulsed Plasma Polymerization of Maleic Anhydride. *Chem. Mater.* **1996**, *8*, 37−42.
(33) Kinmond, E. J.; Coulson, S. R.; Brewer, S. A.; Willis, C.; Badyal, J. P. S. High Structural Retention During Pulsed Plasma Polymerization of 1H,1H,2H-perfluorododecene: an NMR and TOF-SIMS Study. *Polymer* **2005**, *46*, 6829−6835.
(34) Yasuda, H. *Plasma Polymerization*; Academic Press: New York, 1985.
(35) Fonseca, J. L. C.; Apperley, D. C.; Badyal, J. P. S. Plasma Polymerization of Tetramethylsilane. *Chem. Mater.* **1993**, *5*, 1676−1682.
(36) Wood, T. J.; Schofield, W. C. E.; Lund, P.; Larsen, M. J.; Badyal, J. P. S. Highly Ion-Conducting Poly(Ionic Liquid) Layers. *Chem. Commun.* **2012**, *48*, 10201−10203.
(37) Farha, O. K.; Hupp, J. T. Rational Design, Synthesis, Purification, and Activation of Metal-Organic Framework Materials. *Acc. Chem. Res.* **2010**, *43*, 1166−1175.
(38) Evans, J. F.; Gibson, J. H.; Moulder, J. F.; Hammond, J. S.; Goretzki, H. Angle Resolved ESCA Analysis of Plasma Modified Polystyrene. *Fresenius' Z. Anal. Chem.* **1984**, *319*, 841−844.
(39) Johansson, G.; Hedman, J.; Berndtsson, A.; Klasson, M.; Nilsson, R. Calibration of Electron Spectra. *J. Electron Spectrosc. Relat. Phenom.* **1973**, *2*, 295−317.
(40) Kumagai, M.; Tsuchida, K.; Ogino, Y.; Hansen, J.; Ishida, H. Radical Copolymerization of 1-Vinylimidazole and Methacryl- or Styryl-Functional Silane Coupling Agents. *Polymer* **1995**, *36* (3), 535−542.
(41) Lin-Vien, D.; Colthup, N. B.; Fateley, W. G.; Grasselli, J. G. *The Handbook of Infrared and Raman Characteristic Frequencies of Organic Molecules*; Academic Press, Inc.: San Diego, CA, 1991; p 74.
(42) Han, L. M.; Timmons, R. B.; Bogdal, D.; Pielichowski, J. Ring Retention via Pulsed Plasma Polymerization of Heterocyclic Aromatic Compounds. *Chem. Mater.* **1998**, *10*, 1422−1429.
(43) Battjes, K. P.; Barolo, A. M.; Dreyfuss, P. New Evidence Related to Reactions of Aminated Silane Coupling Agents with Carbon Dioxide. *J. Adhes. Sci. Technol.* **1991**, *5* (10), 785−799.
(44) Morris, W.; Leung, B.; Furukawa, H.; Yaghi, O. K.; He, N.; Hayashi, H.; Houndonougbo, Y.; Asta, M.; Laird, B. B.; Yaghi, O. M. A. A Combined Experimental-Computational Investigation of Carbon Dioxide Capture in a Series of Isoreticular Zeolitic Imidazolate Frameworks. *J. Am. Chem. Soc.* **2010**, *132* (32), 11006−11008.
(45) Zaera, F. New Advances in the Use of Infrared Absorption Spectroscopy for the Characterization of Heterogeneous Catalytic Reactions. *Chem. Soc. Rev.* **2014**, *43*, 7624−7663.
(46) Luo, X. F.; Goh, S. H.; Lee, S. Y.; Huan, C. H. A. Spectroscopic Studies of Interactions in Complexes of Poly(1-Vinylimidazole) with Poly(Styrenesulfonic Acid) or the Zinc Salt of Poly(Styrenesulfonate). *Macromol. Chem. Phys.* **1999**, *200*, 874−880.
(47) Lin-Vien, D.; Colthup, N. B.; Fateley, W. G.; Grasselli, J. G. *The Handbook of Infrared and Raman Characteristic Frequencies of Organic Molecules*; Academic Press, Inc.: San Diego, 1991.
(48) Yost, E. C.; Tejedor-Tejedor, M. I.; Anderson, M. A. In Situ CIR-FTIR Characterization of Salicylate Complexes at the Goethite/Aqueous Solution Interface. *Environ. Sci. Technol.* **1990**, *24*, 822−828.
(49) Tranchemontagne, D. J.; Hunt, J. R.; Yaghi, O. M. Room Temperature Synthesis of Metal-Organic Frameworks: MOF-5, MOF-74, MOF-177, MOF-199, and IRMOF-0. *Tetrahedron* **2008**, *64*, 8553−8557.
(50) Mistry, B. D. *A Handbook of Spectroscopic Data: Chemistry*; Oxford Book Company: Delhi, India, 2009.
(51) Ruokolainen, J.; Tanner, J.; ten Brinke, G.; Ikkala, O.; Torkkeli, M.; Serimaa, R. Poly(4-vinyl pyridine)/Zinc Dodecyl Benzene Sulfonate Mesomorphic State Due to Coordination Complexation. *Macromolecules* **1995**, *28*, 7779−7784.
(52) Shirazi, F.; Akhbari, K. Solid-State Thermal Conversion of a Nanoporous Metal−Organic Framework to a Nonporous Coordination Polymer. *RSC Adv.* **2015**, *5*, 50778−50782.
(53) Banh, H.; Gemel, C.; Seidel, R. W.; Fischer, R. A. A Solvated Zinc Analogue of the Calomel-Dication. *Chem. Commun.* **2015**, *51*, 2170−2172.
(54) Mereu, R. A.; Mesaros, A.; Petrisor, T., Jr.; Gabor, M.; Popa, M.; Ciontea, L.; Petrisor, T. Synthesis, Characterization and Thermal Decomposition Study of Zinc Propionate as a Precursor for ZnO Nano-Powders and Thin Films. *J. Anal. Appl. Pyrolysis* **2013**, *104*, 653−659.
(55) Perez, E. V.; Balkus, K. J., Jr.; Ferraris, J. P.; Musselman, I. H. Mixed-Matrix Membranes Containing MOF-5 for Gas Separations. *J. Membr. Sci.* **2009**, *328*, 165−173.
(56) Ferguson, A.; Liu, L.; Tapperwijn, S. J.; Perl, D.; Coudert, F.-X.; Van Cleuvenbergen, S.; Verbiest, T.; van der Veen, M. A.; Telfer, S. G. Controlled Partial Interpenetration in Metal−Organic Frameworks. *Nat. Chem.* **2016**, *8*, 250−257.
(57) NOAA/ESRL Global Monitoring Division. https://www.esrl.noaa.gov/gmd/ccgg/trends/#mlo (accessed June 15, 2017).
(58) Chen, S.; Lin, S.; Chien, R.; Hsu, P. Effects of Shape, Porosity, and Operating Parameters on Carbon Dioxide Recovery in Polytetrafluoroethylene Membranes. *J. Hazard. Mater.* **2010**, *179*, 692−700.
(59) Markov, I. V. *Crystal Growth for Beginners: Fundamentals of Nucleation, Crystal Growth and Epitaxy*; World Scientific Publishing Co. Pte. Ltd.: Singapore, 2003.
(60) Summerfield, A.; Cebula, I.; Schröder, M.; Beton, P. H. Nucleation and Early Stages of Layer-by-Layer Growth of Metal Organic Frameworks on Surfaces. *J. Phys. Chem. C* **2015**, *119*, 23544−23551.
(61) Stavila, V.; Volponi, J.; Katzenmeyer, A. M.; Dixon, M. C.; Allendorf, M. D. Kinetics and Mechanism of Metal−organic Framework Thin Film Growth: Systematic Investigation of HKUST-1 Deposition on QCM Electrodes. *Chem. Sci.* **2012**, *3*, 1531−1540.
(62) Liu, B.; Tu, M.; Fischer, R. A. Metal-Organic Framework Thin Films: Crystallite Orientation Dependent Adsorption. *Angew. Chem., Int. Ed.* **2013**, *52*, 3402−3405.
(63) Gao, W.; Yan, W.; Cai, R.; Williams, K.; Salas, A.; Wojtas, L.; Shi, X.; Ma, S. A Pillared Metal−Organic Framework Incorporated With 1,2,3-Triazole Moieties Exhibiting Remarkable Enhancement Of CO_2 Uptake. *Chem. Commun.* **2012**, *48*, 8898−8900.
(64) Liang, Y.; Harrison, D. P.; Gupta, R. P.; Green, D. A.; McMichael, W. J. Carbon Dioxide Capture Using Dry Sodium-Based Sorbents. *Energy Fuels* **2004**, *18*, 569−575.
(65) Hicks, J. C.; Drese, J. H.; Fauth, D. J.; Gray, M. L.; Qi, G. G.; Jones, C. W. Designing Adsorbents for CO_2 Capture from Flue Gas-Hyperbranched Aminosilicas Capable of Capturing CO_2 Reversibly. *J. Am. Chem. Soc.* **2008**, *130*, 2902−2903.
(66) Simmons, J. M.; Wu, H.; Zhou, W.; Yildirim, T. Carbon Capture in Metal−Organic Frameworks—A Comparative Study. *Energy Environ. Sci.* **2011**, *4*, 2177−2185.
(67) Stolaroff, J. K.; Keith, D. W.; Lowry, G. V. Carbon Dioxide Capture from Atmospheric Air Using Sodium Hydroxide Spray. *Environ. Sci. Technol.* **2008**, *42*, 2728−2735.

DOI: 10.1021/acsami.7b16029
ACS Appl. Mater. Interfaces XXXX, XXX, XXX−XXX

(68) Stuckert, N. R.; Yang, R. T. CO_2 Capture from the Atmosphere and Simultaneous Concentration Using Zeolites and Amine-Grafted SBA-15. *Environ. Sci. Technol.* **2011**, *45*, 10257−10264.
(69) Shekhah, O.; Belmabkhout, Y.; Chen, Z.; Guillerm, V.; Cairns, A.; Adil, K.; Eddaoudi, M. Made-to-Order Metal-Organic Frameworks for Trace Carbon Dioxide Removal and Air Capture. *Nat. Commun.* **2014**, *5*, 4228.
(70) Schneemann, A.; Bon, V.; Schwedler, I.; Senkovska, I.; Kaskel, S.; Fischer, R. A. Flexible Metal−Organic Frameworks. *Chem. Soc. Rev.* **2014**, *43*, 6062−6096.

DOI: 10.1021/acsami.7b16029
ACS Appl. Mater. Interfaces XXXX, XXX, XXX−XXX